Chiral Carbon Dots Synthesized on Cellulose Nanocrystals

Mahshid Chekini, Elisabeth Prince, Lily Zhao, Haridas Mundoor, Ivan I. Smalyukh, and Eugenia Kumacheva*

Hybrid nanoparticles composed of cellulose nanocrystals (CNCs) and carbon-dots (C-dots) have promising applications in chemistry, biology, and nanomedicine, owing to the photoluminescence, sensory properties, and cytocompatibility of C-dots, and chirality, cytobiocompatibility, and high cellular uptake of CNCs. The possibility of circularly polarized luminescence in such nanoparticles is particularly attractive. Herein, scalable and straightforward hydrothermal synthesis of nitrogen-doped fluorescent C-dots under reflux condition by using CNCs as a carbon source and chiral substrate is reported. Under ultraviolet irradiation, hybrid C-dot/CNC nanoparticles exhibit stronger emission of left-handed, than right-handed, circularly polarized light, with high dissymmetry factor up to 0.2. The nanoparticles are biocompatible: the normalized proliferation index above 100% is determined for MCF 7 cells cultured in the suspension of C-dot/CNC nanoparticles. These hybrid nanoparticles can find applications as biotags for labeling, sensing, and therapeutics and as building blocks of photoluminescent cholesteric CNC films with photonic applications.

1. Introduction

Over the past 20 years, synthesis, assembly, and fabrication of chiral (Ch) nanostructures have been motivated by their size-, shape-, and composition-dependent chiroptical properties and promising applications.[1] In particular, nanostructures exhibiting

circularly polarized luminescence (CPL) are sought after in biosensing[2,3] and display technologies,[4,5] telecommunication,[6] and catalysis.[7] For instance, enantioselective interactions of Ch analytes with chiroptical nanomaterials exhibiting specific handedness can be translated into changes in the intensity of fluorescence emission and used in sensing applications.[2,3] Enantioselective catalysis can be achieved by photodegradation of a specific enantiomer using CPL, and thus lead to near-enantiopure chemical products.[7] Furthermore, CPL emission can lead to the generation of new optical devices, e.g., polarizer-free reflective display devices.[4,5] On the other hand, chirality can prompt the formation of stable topologically nontrivial structures, e.g., stable knotted vortices and solitons and even 3D crystals of such knots,[8] which can be potentially utilized as photonic lattices to further enhance and control CPL.

Chirality in man-made nanostructures can be introduced by Ch ligands or substrate during NPs synthesis or assembly, respectively.[9,10] Since a well-defined handedness of small biological molecules (L-amino acids and D-sugars) leads to the affluence of Ch macromolecules and supramolecular structures, e.g., DNA, proteins, or amyloid fibers,[11,12] these species have been successfully employed as substrate for the synthesis or assembly of nanoparticles (NPs).[13] Since the first report on the synthesis of Ag NPs on DNA molecules,[14] a variety of Ch substrate of a biological origin have been employed to translate their chirality into chiroptical properties of NPs, e.g., plasmonic properties of metal NPs[10,15–17] and excitonic properties of semiconductor NPs.[18,19]

Cellulose is one of the most abundant biopolymers.[20] At the molecular level, it consists of polymerized D-glucose units that are linked in linear polymer molecules.[21] These macromolecules organize into fibrous structures with alternating amorphous and crystalline segments.[22] Acid-based hydrolysis of cellulose nanofibers yields whisker-shaped 100–300 nm long cellulose nanocrystals (CNCs),[23,24] which exhibit a right-handed twist along their long axis.[25–29] Furthermore, in aqueous suspensions CNCs form lyotropic left-handed Ch nematic liquid crystals.[30–34]

Research on the development of CNCs-derived materials is motivated by their biocompatibility, relatively low-cost, sustainability, the ease of surface functionalization of CNCs, and a Ch nematic structure of CNC films.[31,35,36] Functional nanomaterials have been generated using CNCs as structural support for

Dr. M. Chekini, E. Prince, L. Zhao, Prof. E. Kumacheva
Department of Chemistry
University of Toronto
80 Saint George Street, Toronto, ON M5S 3H6, Canada
E-mail: eugenia.kumacheva@utoronto.ca
Dr. H. Mundoor, Prof. I. I. Smalyukh
Department of Physics and Soft Materials Research Center
University of Colorado
Boulder, CO 80309, USA
Prof. I. I. Smalyukh
Department of Electrical
Computer, and Energy Engineering
Materials Science and Engineering Program
University of Colorado
Boulder, CO 80309, USA
Prof. E. Kumacheva
Department of Chemical Engineering and Applied Chemistry
University of Toronto
Toronto, ON M5S 3E5, Canada

the synthesis of catalytically active metal gold and palladium NPs,[37,38] and deposition of semiconductor[39] or metal NPs.[40]

Recently, carbon nanoparticles (carbon dots, C-dots) have been used in mixtures with CNCs to fabricate iridescent and luminescent left-handed Ch nematic films.[41–43] Control of CPL was achieved by superimposing a photoluminescence band of C-dots and a photonic bandgap of the Ch-CNC host, thus making composite films behave as a polarized light filter or sensor.[43] Individual hybrid NPs comprised of C-dots and CNCs have not been reported, although in suspensions they can combine the photoluminescence, sensory properties, and cytocompatibility of C-dots, and chirality, cytobiocompatibility, and high cellular uptake of CNCs.[44]

Here we used individual CNCs as a carbon source and as a twisted substrate for C-dots synthesis to generate hybrid C-dot/CNC NPs. Being motivated by successful C-dots synthesis using D-glucose molecules as carbon source,[45–48] we synthesized C-dots by using hydrolyzed sugar moieties on the CNC surface as a carbon source. These surface glucose moieties reacted with ethylenediamine, as N source for doping of C-dots. Hybrid C-dot/CNC NPs exhibited absorption in the UV spectral region and photoluminescence emission in the visible spectral region. More interestingly, photoluminescence emission of C-dot/CNC NPs exhibited dissymmetry, with enhanced left-handed CPL emission. We can benefit from the CPL emission of NPs in bioimaging applications. By using NPs with CPL emission as biotag for cell labeling we can introduce a new strategy for bioimaging, using circularly polarized fluorescence microscopy, which can help to further eliminate the background photoluminescence and enhance image quality. Cell viability assay showed that these NPs are noncytotoxic, thus suggesting that they can be used as biotags and in drug delivery applications.

2. Results and Discussion

Figure 1 illustrates schematically the synthesis of C-dots on the CNC surface. Following the addition of ethylenediamine and boric acid to an aqueous CNC suspension (Step 1), the reaction mixture was maintained under reflux conditions for the time interval varying from 3 to 48 h (Step 2). Subsequently to that, the suspension was cooled down to room temperature and dialyzed against Milli-Q-grade deionized water (DI, 18.2 MΩ cm resistivity) for 5 days with water replacement three times per day (Step 3). The recipe for C-dot synthesis on the CNCs surface is provided in the Experimental Section. We note that C-dot synthesis under reflux conditions was preferred over a more cost-effective and environmentally friendly hydrothermal C-dot synthesis, as the latter resulted in the loss of structural integrity of CNCs.

Figure 2 shows transmission electron microscopy (TEM) images of CNCs after different reaction durations. In comparison with pristine CNCs (Figure 2a), small NPs with high electron density appeared on the CNCs surface after 6 and 12 h long reaction (Figure 2b,c, respectively). The corresponding average NP size was 1.6 ± 0.9 and 2.8 ± 2.3 nm (see the histograms in Figure S1, Supporting Information). Longer reaction duration resulted in larger NP size, a broader NP size distribution, and a higher NP density on the CNC surface (Figures S1 and S2, Supporting Information). The presence of NPs on the surface of well-dispersed CNCs further minimizes the aggregation potential, however, the synthesis induces some aggregation and length increase in the CNCs after the synthesis (Figure S3, Supporting Information). With an increase of the reaction time to 18 h, the NPs detached from the CNCs surface and aggregated (Figure 2d), and after 21 h, the CNCs lost their integrity and decomposed.

Next, we examined the elemental composition of hybrid NPs after 6 h synthesis (as in Figure 2b). The CNCs prior to the reaction were used as a reference system. The XPS spectra in **Figure 3** and the results of elemental analysis (summarized in Tables S1 and S2, Supporting Information), indicated that the main elements of the CNCs and hybrid NPs were C and O. Following the reflux reaction, the C/O ratio increased from 1.27 to 1.58, while the amount of N increased approximately from 0.19 to 0.79 at%, that is, fourfold, in comparison with pristine CNCs. Thus, we conclude that hydrothermal synthesis under reflux conditions resulted in the formation of N-doped C-dots. Similar to the C-dot synthesis from citric acid and ethylenediamine,[48–51] wherein the citric acid reacts and condenses with ethylenediamine, the surface glucose moieties on the CNC surface reacted with ethylenediamine and formed C-dots under reflux condition. In addition to being a nitrogen source for C-dots doping, ethylenediamine facilitated the
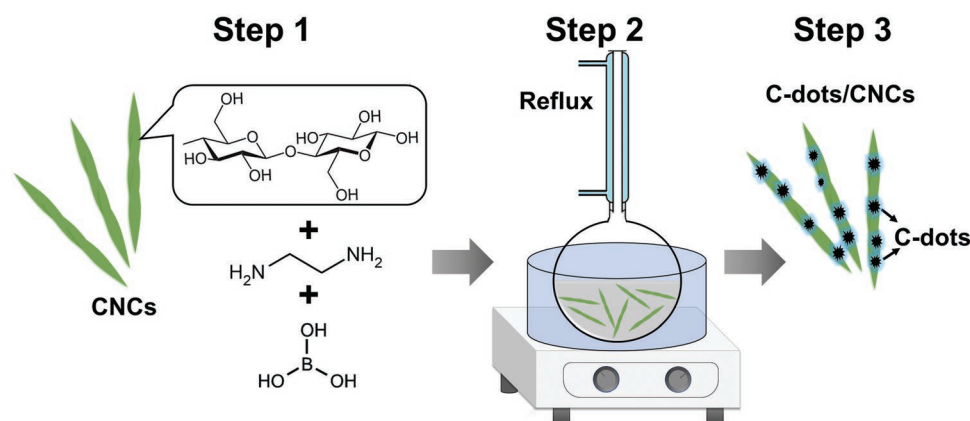
Figure 1. Schematic of C-dot synthesis on the CNC surface.

**ADVANCED
SCIENCE NEWS**
www.advancedsciencenews.com

**ADVANCED
OPTICAL
MATERIALS**
www.advopticalmat.de
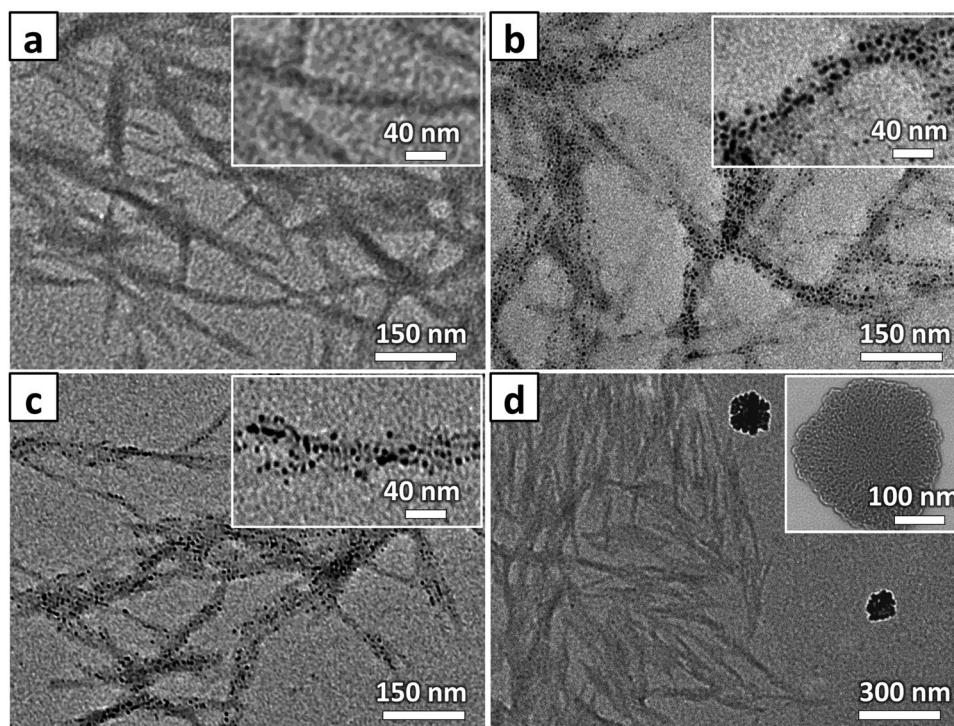
Figure 2. TEM images of CNCs a) prior to and b) after 6, c) 12, and d) 18 h synthesis. Insets in (a–c) show corresponding high-magnification TEM images. Inset in (d) shows an aggregate of NPs detached from the CNC surface.

condensation/polymerization reaction. Notably, while C-dots were formed in the presence of ethylenediamine (or triethylenediamine) the use of other amine-containing molecules such as diethylenetriamine, urea, p-phenylenediamine, o-phenylenediamine, cysteamine, and thiourea did not result in C-dot synthesis (Table S3, Supporting Information).
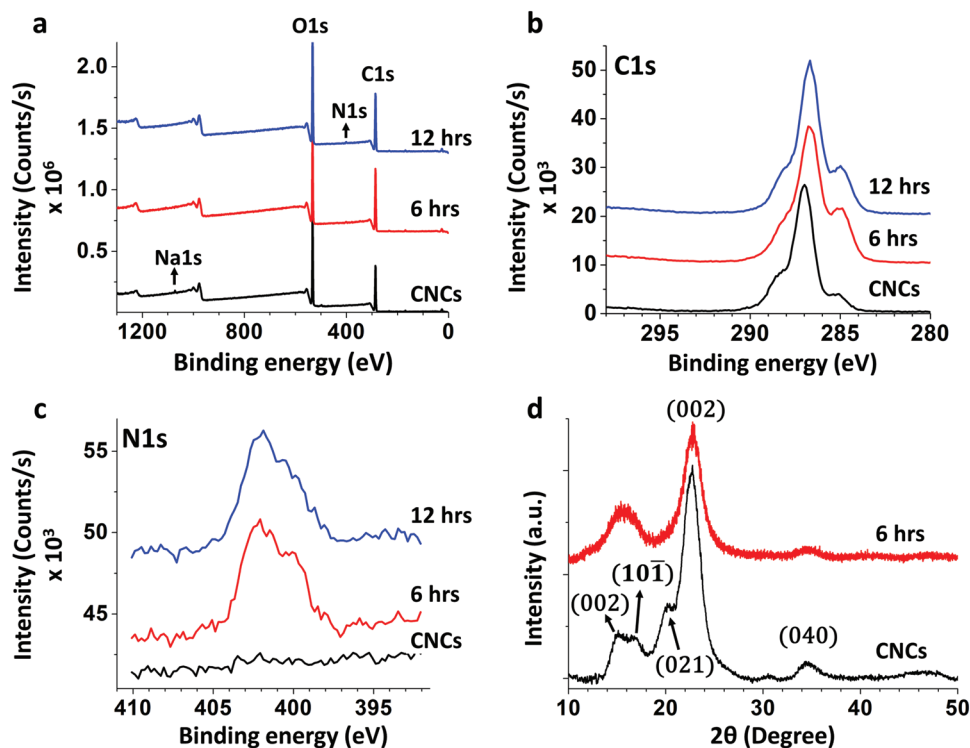
Figure 3. Characterization of hybrid NPs using XPS and XRD. a) XPS survey spectra. b,c) High-resolution C1s and N1s XPS spectra of CNCs and hybrid NPs after 6 and 12 h C-dot synthesis. d) XRD spectra of CNCs and hybrid NPs after 6 h C-dot synthesis.

**ADVANCED
SCIENCE NEWS**

www.advancedsciencenews.com

**ADVANCED
OPTICAL
MATERIALS**

www.advopticalmat.de

We note that although in our work, boric acid could provide a source of boron,[48] no significant B doping was observed for C-dots, even after 12 h reaction (Figure 3).[48] Presumably, mild reaction conditions used in our work did not provide the energy required for the condensation and incorporation of B into the molecular structure of C-dots. Elimination of boric acid from the reaction resulted in a notable decrease in the reaction rate, judged by the change in color of the reaction mixture and evolution of photoluminescence. We speculate that boric acid could act as a catalyst in the condensation and polymerization reactions.[52–54]

Importantly, replacement of CNCs with cellulose nanofibers (CNFs) resulted in a very slow reaction, with C-dot formation only after 18 h. We ascribe the difference in CNC and CNF reactivity to CNC preparation by the sulfuric acid hydrolysis, leading to broken bonds in cellulose molecules on the CNC surface and generating negatively charged surface sulfate groups. The difference in the surface chemistry, as well as a reduced thermal stability and larger surface area of CNCs made them more amenable to the C-dots synthesis, that is condensation (removal of water molecules), polymerization (crosslinking), and carbonization.[50,55–57]

Mild reaction conditions were essential for keeping CNCs integrity during the synthesis of C-dots. The X-ray diffraction (XRD) results in Figure 3d show that the crystalline structure of CNCs was affected by the reaction: the intensity of diffraction peaks decreased and the fine features of the spectrum (for $10 \leq 2\theta \leq 20°$) disappeared after 6 h C-dot synthesis. The ratio of the main crystalline peak (002) intensity to the background (crystallinity index) reduced from 89% to 80%. This gradual decrease in crystalline structure is in agreement with the results of TEM imaging of hybrid NPs, that is, the loss of integrity of CNCs after the prolonged reaction. For crystalline C-dots the diffraction peaks were expected for 2θ in the 10°–40° region, which overlaps with the CNC peaks, however, we did not expect the formation of crystalline C-dots, due to the mild reaction conditions.[50,55–57]

Figure 4 shows the extinction and photoluminescence (PL) properties of aqueous C-dot/CNC NP suspensions after different synthesis duration. Under reflux conditions, the color of the suspension monitored under white light illumination changed from white (prior to the reaction) to yellow (Figure 4a, top). The original UV–vis extinction spectra of the suspension exhibited a typical scattering pattern, with no characteristic absorption in the 200–700 nm spectral region. Following C-dot synthesis, two absorption peaks at 307 and 380 nm emerged in the spectra, with peak intensity increasing at longer reaction time, due to the formation of a larger number of C-dots with a greater size. The absorption peaks in the 300–400 nm spectral region were attributed to the low energy transitions (wavelengths ≈ 300 nm and above) in C-dots, caused by n–π* transitions in carbonyl groups,[48,58] functional surface states, or other fluorophore-like molecular surface states.[48,50,57] Since no absorption peak corresponding to the core state (π–π*) and edge state (n–π*) transitions[57] existed in the 200–300 nm spectral region, we conclude that the main contributions in absorbance were generated from C-dot surface states.

Figure 4b, top shows the photographs of the C-dot/CNC NP suspensions, taken under illumination at 365 nm. The intensity of PL in the suspensions increased with increasing duration of C-dot synthesis (top inset). Figure 4b, bottom shows the PL spectra of the C-dot/CNC NP suspensions after varying synthesis time. The PL emission intensity increased with reaction duration, due to a higher content of C-dots. Moreover, the spectral position of PL peak shifted from 461 nm (3 h reaction) to 468 nm (21 h reaction), due to the formation of larger C-dots and their aggregation. Increasing the duration of C-dot synthesis from 21 to 48 h resulted in PL intensity reduction, due to the PL self-quenching, as a result of aggregation of C-dots, as well as hybrid nanoparticles. Dilution of the C-dot/CNC suspension after 48 h C-dot synthesis resulted in the increase in PL intensity (Figure S5, Supporting Information). The autofluorescence of CNCs (small peaks in the 400–500 nm region) was ascribed to lignin impurities.[59] Based on the results of TEM imaging and XRD experiments, long C-dot synthesis duration resulted in CNC disintegration, thus in the rest of our work we focused on the C-dot/CNC NPs synthesized during 6 h reaction.
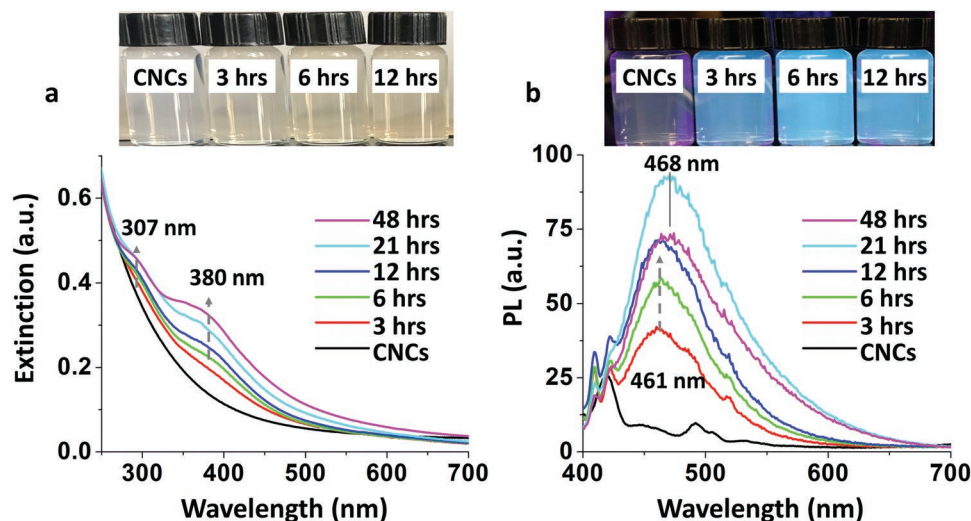
Figure 4. a) Extinction and b) PL spectra of C-dot/CNC NP suspensions, following different reaction times. The photographs of the suspensions under white light illumination and irradiation at 365 nm are shown in the corresponding insets.

**ADVANCED
SCIENCE NEWS**

www.advancedsciencenews.com

**ADVANCED
OPTICAL
MATERIALS**

www.advopticalmat.de
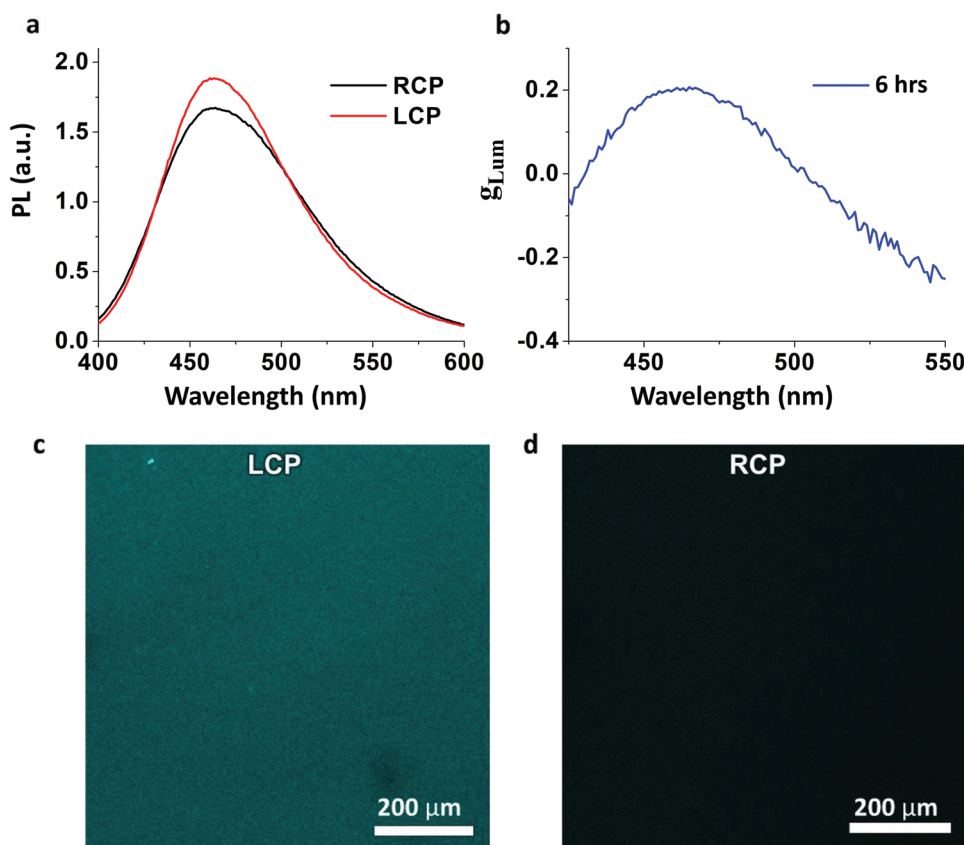
Figure 5. a) Photoluminescence spectra of the C-dot/CNC suspensions after 6 h C-dot synthesis, recorded using left- and right-handed circular polarizers (LCP and RCP, respectively). b) The variation in the calculated g_{Lum} plotted as a function of emission wavelength. The confocal fluorescence microscopy images of NPs suspension under c) LCP and d) RCP, imaged using DAPI channel (405 nm excitation) while the microscope settings such as gain, exposure time, and laser intensity were maintained the same.

Figure 5a shows the PL emission spectra of C-dot/CNC NP suspension after 6 h C-dot synthesis. The spectra were acquired under left- and right-handed circular polarizers (LCP and RCP, respectively). At 460 nm, the intensity of the emitted light with left-handed circular polarization was ≈12% higher than that with right-handed circular polarization.

Based on the difference in the LCP and RCP spectra, the dissymmetry factor was calculated as

$$g_{Lum} = 2(I_L - I_R)/(I_L + I_R) \qquad (1)$$

where I_L and I_R are the intensities of the left- and right-handed CPL, respectively.

Figure 5b shows the variation in g_{Lum}, plotted as a function of the emission wavelength for the C-dot/CNC NP suspension after 6 h C-dot synthesis, calculated from the spectra in Figure 5a. The value of the g_{Lum} at 460 nm (the wavelength corresponding to the maximum emission intensity) was 0.2, that is, significantly higher than the reported values for dye/CNC hybrids, e.g., g_{Lum} of 3.3×10^{-2} for pyrene/CNC hybrid obtained by Ch induction.[60] Notably, the value of g_{Lum} at 460 nm for C-dot/CNC suspension was as high as some of the highest values reported for the Ch-CNC composite films obtained from mixtures of CNCs with NPs (−0.2)[42] or dyes (−0.28).[61] The origins of CPL in Ch-CNC films and C-dot/CNC suspension in our work is different: films effectively block L-CPL

transmission and emission, which results in R-CPL emission with negative g_{Lum} values,[62,63] while in our work, the L-CPL emission was stronger and g_{Lum} was positive, due to the Ch induction or Ch nature of C-dots themselves. We also note that the circular dichroism spectra (CD) spectra prior to and after C-dot synthesis in Figure S7 (Supporting Information) show no significant difference in the CD spectra.

For inorganic NPs deposited on the CNCs surface, chirality can be induced by their Ch organization along the twisted CNCs[40] or chirality induction from glucose units acting as NP ligands. No reports exist on the chirality induction and chiroptical properties of hybrid C-dot/CNC NPs, neither due to C-dot geometrical arrangement, nor owing to the chirality induction. Notably, the challenge in the bottom-to-top synthesis of Ch C-dots (and graphene quantum dots) stems from the loss of chirality and racemization under harsh reaction conditions, e.g., high temperatures.[64,65] The mild reaction conditions selected in our work enabled the transfer of the chirality of the CNC moieties to C-dots.

Figure 5c,d shows confocal fluorescence microscopy images of the suspension of C-dot/CNC NPs under LCP and RCP, respectively, with a significantly brighter image taken under LCP. Importantly, these images were taken at the same spot of the sample by maintaining the same settings on the microscope (see the Experimental Section). The favorable left-handed

**ADVANCED
SCIENCE NEWS**
www.advancedsciencenews.com

**ADVANCED
OPTICAL
MATERIALS**
www.advopticalmat.de
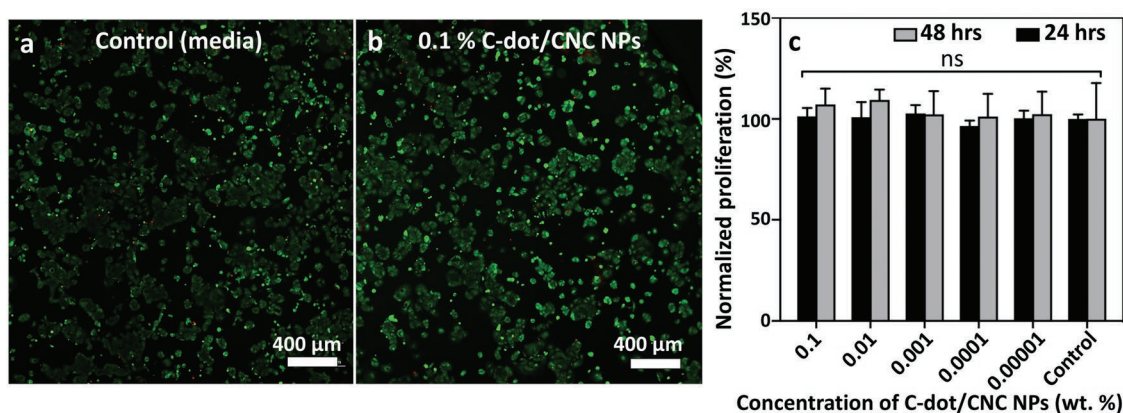
Figure 6. Examination of biocompatibility of C-dot/CNC NPs. a,b) Fluorescence microscopy images of the live (calcein-AM stained, green) and dead (ethidium homodimer stained, red) MCF 7 cells after 48 h of cell culture. (a) MCF 7 cells in the control system (without exposure to the C-dot/CNC NPs). (b) MCF 7 cells cultured in the 0.1 wt% suspension of C-dot/CNC NPs. c) Normalized proliferation index of MCF-7 cells cultured in suspensions with different concentrations of C-dot/CNC NPs, measured by the PrestoBlue assay after 24 (black bars) and 48 h (gray bars). The error bar is mean ± standard deviation ($N = 3$). *ns: $p > 0.1$ from Student's t-test with Bonferroni correction.

CPL emission of the hybrid C-dot/CNC NPs can open a way for enhancing the quality of imaging of biological species by suppressing background PL signal, due to, e.g., autofluorescence in the 400–550 nm spectral range.[66]

There is a growing interest in using CNCs in nanomedicine, due to their biocompatibility,[67–69] as well as their asymmetric (rod-like) shape facilitating prolonged blood circulation time and possible cellular uptake.[70–72] Furthermore, the hydroxyl groups on the CNCs surface are amenable for attachment of polymer molecules[68,73] or imaging and therapeutic agents.[74,75] Since C-dot/CNC NPs can be used as biotags for labeling, sensing, and therapeutics, we examined their biocompatibility by culturing MCF-7 breast cancer cells for 24 and 48 h in suspensions of hybrid NPs with concentrations from 0.00001 to 0.1 wt% in cell culture media. Notably, the highest tested concentration was at least, tenfold higher than the highest concentration tested for biocompatibility of composite CNC NPs.[44,72,74–76] In the control experiment, the cells were cultured in the cell culture media without exposure to C-dot/CNC NPs. **Figure 6**a,b shows the fluorescence microscopy images of the live (calcein-AM stained, green) and dead (ethidium homodimer stained, red) cells after 48 h of cell culture for the control system and with exposure to 0.1 wt% C-dot/CNC NPs (the fluorescence microscopy images for suspensions with other concentrations are shown in Figure S8, Supporting Information). Cell viability was quantified by the PrestoBlue assay. The normalized proliferation index determined as the ratio of Resazurin (PrestoBlue) fluorescence intensity at $\lambda_{max} = 590$ nm under excitation at 540 nm, relative to the control system. The fluorescence intensity values were normalized to the intensity of the control system at the same cell culture duration. We note that under this excitation and emission wavelengths, absorption, and emission of hybrid C-dot/CNC NPs were negligible.

Figure 6c shows the normalized proliferation index, at 24 and 48 h of cell culture. The proliferation index after 48 h varied from 100% ± 17% to 107% ± 8%. No statistically significant difference in the normalized proliferation index existed upon cell exposure to suspensions with different concentrations of C-dot/CNC NPs and the control system over both 24 and 48 h of cell culture. Therefore, we conclude that no cytotoxicity of C-dot/CNC NPs was observed during 24 and 48 h of cell culture, even for NP concentration as high as 0.1 wt%.

3. Conclusion

We report a facile and scalable method for the synthesis of Ch photoluminescent N-doped C-dots on the surface of CNCs. The CNCs acted as a carbon source and a Ch substrate. The geometrical arrangement of C-dots on the twisted CNC surface did not induce chirality in the optical properties of the C-dots, however their chirality could originate from the preservation of molecular chirality of the CNC surface glucose units under mild synthesis conditions. The PL spectra recorded under left- and right-handed circular polarizers showed a higher intensity of left-handed CPL of hybrid C-dot/CNC NPs. The anisotropy factor, $g_{Lum} = 0.2$ at the maximum emission wavelength was significantly higher than the reported values for hybrid CNC NPs. Confocal fluorescence microscopy imaging using circular polarizers and staining using the Ch NPs with CPL emission enables effective elimination of the PL background and improves the signal-to-noise ratio. Cell viability tests showed that C-dot/CNC NPs were not cytotoxic and the normalized proliferation index was above 100% upon MCF 7 cell exposure to the C-dot/CNC NP suspensions with NP concentration up to 0.1 wt%. These C-dot/CNC NPs have applications as biocompatible Ch nanolabels, with the possibility to provide CPL for bioimaging. Due to NPs cytocompatibility, they can be effective in bioimaging besides their applications in targeting, sensing and as drug-delivery agents. Furthermore, since the CNCs self-organize into 1D photonic crystal lattices, these hybrid C-dot/CNC NPs may enable the fabrication of distributed-feedback mirror-free cholesteric lasers,[77] and achieve the solar gain control, due to the combination of near-infrared reflectivity and visible emission, to develop new breeds of solar concentrator for smart windows and other applications.[78]

4. Experimental Section

Materials: An aqueous CNCs suspension (12.2 wt%) and CNF (3 wt%) were supplied by the University of Maine Process Development Center. Boric acid (≥99.5%, ReagentPlus), ethylenediamine (≥99.5%, ReagentPlus), diethylenetriamine (≥90%, ReagentPlus), urea (≥98%, BioReagent), p-phenylenediamine (98%), o-phenylenediamine (99.5%), cysteamine (98%), and thiourea (≥99%, ReagentPlus) were purchased from Sigma-Aldrich, Canada. The cellulose membrane dialysis tubing with molecular weight 14 kDa cut-off was purchased from Sigma-Aldrich, Canada. PrestoBlue Cell Viability Reagent was supplied by Life Technologies. Calcein-AM and ethidium homodimer stains were purchased from Invitrogen. Milli-Q grade deionized water (DI, 18.2 MΩ cm resistivity) was used in all experiments.

Synthesis of C-Dot/CNC NPs: 10 mmol of boric acid was dissolved in 50 mL of 2 wt% CNCs suspension in DI water in a round-bottom flask under stirring. To the mixed suspension of boric acid and CNCs, 10.4 mmol of ethylenediamine was added under vigorous stirring. The flask was transferred into a preheated oil bath at 110 °C and maintained under reflux conditions for different time intervals.

Synthesis of C-Dot/CNC NPs Using Other Reactants Than Ethylenediamine: Ethylenediamine was replaced by an equivalent molar-amount of diethylenetriamine, urea, p-phenylenediamine, o-phenylenediamine, cysteamine, thiourea or a mixture of ethylenediamine and p-phenylenediamine, while the rest of the recipe was maintained similar to the synthesis of C-dot/CNC NPs with ethylenediamine (Section S3, Supporting Information). Each reaction was monitored for up to 12 h by measuring the intensity of PL emission.

Characterization Methods: TEM images were acquired using a Hitachi HT7700 microscope at 85 kV. The average size and distance between the C-dots were determined by analyzing TEM images using the ImageJ software (ImageJ, US National Institutes of Health, Bethesda, MA, USA). The distribution of C-dot dimensions and interparticle distance were determined by analyzing 400 and 230 C-dots after for 6 and 12 h synthesis, respectively. The X-ray photoelectron spectroscopy (XPS) spectra were collected a Thermofisher Scientific K-Alpha system (Thermofisher Scientific – E. Grinstead, UK) with monochromatic Al Kα radiation (1486 eV). The nominal spot size of 400 µm and 200 eV pass energy was used for survey spectra, 25 eV pass energy and energy steps of 0.1 eV were used for high-resolution measurements. Charge compensation was applied using the system's combined e$^-$/Ar$^+$ flood gun. The energy scale was adjusted to place the most intense C 1s peak (C—O bonding) at 286.7 eV. All data processing was performed using Avantage 5.926 software. The relative atomic composition was obtained from the individual region spectra after subtraction of a Shirley-type background[79] and application of the supplied sensitivity factors. Powder XRD was performed using a Phillips PW1830 XRD system and the diffractograms were recorded using Cu Kα radiation from Cu X-ray tube as an anode with 40 kV voltage and 40 mA current. The measurements were performed for 2θ in the range from 10° to 50° with a scan speed of 1 s per step and a step size of 0.01°. All samples were purified and freeze-dried prior to XRD and XPS measurements.

The Cary 5000 UV–vis–NIR spectrophotometer was used to acquire the extinction spectra of the C-dot/CNC suspension. Varian Cary Eclipse fluorescence spectrophotometer (Agilent Technologies, Santa Clara, CA, USA) was used for recording photoluminescent emission spectra. Jasco J-710 circular dichroism spectrophotometer was used to collect CD spectra.

Circularly polarized photoluminescence measurements were performed using a customized spectrofluorometer system (Horiba Scientific, Fluorolog 3), equipped with high-resolution excitation and emission monochromators (1200 g mm^{-1}). The aqueous dispersions of C-dot/CNC were transferred to a quartz cuvette and loaded into the sample holder. The samples were excited with a 365 nm linear polarized light from a xenon lamp and the emission signal from the sample was sent to the monochromator and a photomultiplier tube positioned orthogonally to the excitation direction. The left and right circularly polarized components (LCP, RCP) of the photoluminescence signal were separated using an achromatic quarter waveplate and a broadband polarizer placed after the sample holder. Based on these measurements the dissymmetry factor g_{Lum} was calculated using Equation (1). To prevent artifacts associated with the presence of linear polarized components in the emission, the polarization state of the excitation beam was kept parallel to the detection direction. The measurements were performed with an average excitation power of 3.6 mW and the corresponding power density was estimated to be 15 mW cm^{-2}.

Cell Culture and Viability Assay: MCF-7 breast cancer cells of human origin were cultured on tissue culture polystyrene at 37 °C and in 5% of CO_2, using Dulbecco's Eagle's minimum essential media supplemented with 10% fetal bovine serum (Atlanta Biologics), 5 mg of insulin, and 1% penicillin–streptomycin–amphotericin (MediaTech Inc.). Every 4–5 days, a 0.25 wt% Trypsin-EDTA solution (GIBCO) was used to detach the cells from the plastic flask. After cell detachment, fresh nutrition medium was added, and the cell suspension was centrifuged at 1000 rpm for 3 min. The supernatant was then removed, and the cell suspension was redispersed in a fresh medium.

To examine the cytotoxicity of C-dot/CNC NPs, cells were cultured in the nutrition media in the presence and absence of C-dot/CNC NPs. Cells were plated at a cell density of 100 cell µL in 96 well plates (100 µL, 100 cells per well), and allowed to settle for 24 h. A solution of pure cell culture media (control system) or C-dot/CNC NPs in the cell culture media was then added to the wells. The cell viability was examined by PrestoBlue assay (Life Technologies) and the growth kinetics was monitored after 24 and 48 h. PrestoBlue reagent with 10% w/w concentration was applied to the culture media. The viability of the cells was quantified by fluorescence measurements (Bio-Tek Synergy HT, with excitation and emission at 540 and 590 nm, respectively) after 1 h of incubation on 100 mL supernatant in a 96-well plate. Higher metabolic activity was indicated by the higher fluorescence intensity values. The normalized proliferation index was defined as the fluorescence intensity of the cell suspension in the presence of C-dot/CNC NPs divided by the fluorescence intensity of the control sample with the same cell culture duration.

Confocal Microscopy Imaging: The fluorescence images were obtained by a Zeiss LSM700 confocal microscope. The NPs were imaged using DAPI channel (laser excitation at 405 nm), 4× objective and microscope settings (gain, exposure time, and laser intensity) were maintained the same for the sample of interest and the control system.

Supporting Information

Supporting Information is available from the Wiley Online Library or from the author.

Acknowledgements

Conflict of Interest

The authors declare no conflict of interest.

Keywords

[1] W. Ma, L. Xu, A. F. de Moura, X. Wu, H. Kuang, C. Xu, N. A. Kotov, *Chem. Rev.* **2017**, *117*, 8041.
[2] C. Han, H. Li, *Small* **2008**, *4*, 1344.
[3] C. Carrillo-Carrión, S. Cárdenas, B. M. Simonet, M. Valcárcel, *Anal. Chem.* **2009**, *81*, 4730.
[4] H. Maeda, Y. Bando, K. Shimomura, I. Yamada, M. Naito, K. Nobusawa, H. Tsumatori, T. Kawai, *J. Am. Chem. Soc.* **2011**, *133*, 9266.
[5] D. Zhao, H. He, X. Gu, L. Guo, K. S. Wong, J. W. Y. Lam, B. Z. Tang, *Adv. Opt. Mater.* **2016**, *4*, 534.
[6] Y. Yang, R. C. da Costa, M. J. Fuchter, A. J. Campbell, *Nat. Photonics* **2013**, *7*, 634.
[7] T. Kawasaki, M. Sato, S. Ishiguro, T. Saito, Y. Morishita, I. Sato, H. Nishino, Y. Inoue, K. Soai, *J. Am. Chem. Soc.* **2005**, *127*, 3274.
[8] J.-S. B. Tai, I. I. Smalyukh, *Science* **2019**, *365*, 1449.
[9] S. . Gallagher, M. P. Moloney, M. Wojdyla, S. J. Quinn, J. M. Kelly, Y. K. Gun'ko, *J. Mater. Chem.* **2010**, *20*, 8350.
[10] J. M. Slocik, A. O. Govorov, R. R. Naik, *Nano Lett.* **2011**, *11*, 701.
[11] N. Rubin, E. Perugia, M. Goldschmidt, M. Fridkin, L. Addadi, N. Rubin, E. Perugia, M. Goldschmidt, M. Fridkin, L. Addadi, *J. Am. Chem. Soc.* **2008**, *130*, 4602.
[12] D. Hamada, I. Yanagihara, K. Tsumoto, *Trends Biotechnol.* **2004**, *22*, 93.
[13] J. Kumar, L. M. Liz-Marzán, *Bull. Chem. Soc. Jpn.* **2019**, *92*, 30.
[14] G. Shemer, O. Krichevski, G. Markovich, T. Molotsky, I. Lubitz, A. B. Kotlyar, *J. Am. Chem. Soc.* **2006**, *128*, 11006.
[15] A. Kuzyk, R. Schreiber, Z. Fan, G. Pardatscher, E.-M. Roller, A. Högele, F. C. Simmel, A. O. Govorov, T. Liedl, *Nature* **2012**, *483*, 311.
[16] A. G. Mark, J. G. Gibbs, T.-C. Lee, P. Fischer, *Nat. Mater.* **2013**, *12*, 802.
[17] A. Guerrero-Martínez, J. L. Alonso-Gómez, B. Auguié, M. M. Cid, L. M. Liz-Marzán, *Nano Today* **2011**, *6*, 381.
[18] E. D. Sone, E. R. Zubarev, S. I. Stupp, *Angew. Chem., Int. Ed.* **2002**, *41*, 1705.
[19] S. Huo, P. Duan, T. Jiao, Q. Peng, M. Liu, *Angew. Chem., Int. Ed.* **2017**, *56*, 12174.
[20] T. H. Wegner, P. E. Jones, *Cellulose* **2006**, *13*, 115.
[21] J. Credou, T. Berthelot, *J. Mater. Chem. B* **2014**, *2*, 4767.
[22] R. J. Moon, A. Martini, J. Nairn, J. Simonsen, J. Youngblood, *Chem. Soc. Rev.* **2011**, *40*, 3941.
[23] S. M. Mukherjee, J. Sikorski, H. J. Woods, *J. Text. Inst. Trans.* **1952**, *43*, T196.
[24] S. M. Mukherjee, H. J. Woods, *Bioch. Biophys. Acta* **1953**, *10*, 499.
[25] I. Usov, G. Nyström, J. Adamcik, S. Handschin, C. Schütz, A. Fall, L. Bergström, R. Mezzenga, *Nat. Commun.* **2015**, *6*, 7564.
[26] K. Conley, M. A. Whitehead, T. G. M. M. van de Ven, *Cellulose* **2017**, *24*, 479.
[27] S. Paavilainen, T. Róg, I. Vattulainen, *J. Phys. Chem. B* **2011**, *115*, 3747.
[28] Z. Zhao, O. E. Shklyaev, A. Nili, M. N. A. Mohamed, J. D. Kubicki, V. H. Crespi, L. Zhong, *J. Phys. Chem. A* **2013**, *117*, 2580.
[29] W. J. Orts, L. Godbout, R. H. Marchessault, J. F. Revol, *Macromolecules* **1998**, *31*, 5717.

[30] E. Fortunati, I. Armentano, Q. Zhou, A. Iannoni, E. Saino, L. Visai, L. A. Berglund, J. M. Kenny, *Carbohydr. Polym.* **2012**, *87*, 1596.
[31] A. Querejeta-Fernández, G. Chauve, M. Methot, J. Bouchard, E. Kumacheva, *J. Am. Chem. Soc.* **2014**, *136*, 4788.
[32] P. Rofouie, M. Alizadehgiashi, H. Mundoor, I. I. Smalyukh, E. Kumacheva, *Adv. Funct. Mater.* **2018**, *28*, 1803852.
[33] P. Rofouie, E. Galati, L. Sun, A. S. Helmy, E. Kumacheva, *Adv. Funct. Mater.* **2019**, *29*, 1905552.
[34] M. Schlesinger, M. Giese, L. K. Blusch, W. Y. Hamad, M. J. MacLachlan, *Chem. Commun.* **2015**, *51*, 530.
[35] K. E. Shopsowitz, H. Qi, W. Y. Hamad, M. J. MacLachlan, *Nature* **2010**, *468*, 422.
[36] A. G. Dumanli, G. Kamita, J. Landman, H. van der Kooij, B. J. Glover, J. J. Baumberg, U. Steiner, S. Vignolini, *Adv. Opt. Mater.* **2014**, *2*, 646.
[37] X. Wu, C. Lu, Z. Zhou, G. Yuan, R. Xiong, X. Zhang, *Environ. Sci.: Nano* **2014**, *1*, 71.
[38] C. M. Cirtiu, A. F. Dunlop-Brière, A. Moores, *Green Chem.* **2011**, *13*, 288.
[39] S. Padalkar, J. R. Capadona, S. J. Rowan, C. Weder, R. J. Moon, L. A. Stanciu, *J. Mater. Sci.* **2011**, *46*, 5672.
[40] J. Majoinen, J. Hassinen, J. S. Haataja, H. T. Rekola, E. Kontturi, M. A. Kostiainen, R. H. A. Ras, P. Törmä, O. Ikkala, *Adv. Mater.* **2016**, *28*, 5262.
[41] E. Lizundia, T. D. Nguyen, J. L. Vilas, W. Y. Hamad, M. J. Maclachlan, *Mater. Chem. Front.* **2017**, *1*, 979.
[42] R. Xiong, S. Yu, M. J. Smith, J. Zhou, M. Krecker, L. Zhang, D. Nepal, T. J. Bunning, V. V. Tsukruk, *ACS Nano* **2019**, *13*, 9074.
[43] H. Zheng, B. Ju, X. Wang, W. Wang, M. Li, Z. Tang, S. X.-A. Zhang, Y. Xu, *Adv. Opt. Mater.* **2018**, *6*, 1801246.
[44] J. Guo, D. Liu, I. Filpponen, L.-S. Johansson, J.-M. Malho, S. Quraishi, F. Liebner, H. A. Santos, O. J. Rojas, *Biomacromolecules* **2017**, *18*, 2045.
[45] Z.-C. C. Yang, M. Wang, A. M. Yong, S. Y. Wong, X.-H. H. Zhang, H. Tan, A. Y. Chang, X. Li, J. Wang, *Chem. Commun.* **2011**, *47*, 11615.
[46] Z. Ma, H. Ming, H. Huang, Y. Liu, Z. Kang, *New J. Chem.* **2012**, *36*, 861.
[47] H. Peng, J. Travas-Sejdic, *Chem. Mater.* **2009**, *21*, 5563.
[48] Y. Choi, B. Kang, J. Lee, S. Kim, G. T. Kim, H. Kang, B. R. Lee, H. Kim, S.-H. Shim, G. Lee, O.-H. Kwon, B.-S. Kim, *Chem. Mater.* **2016**, *28*, 6840.
[49] S. Zhu, Q. Meng, L. Wang, J. Zhang, Y. Song, H. Jin, K. Zhang, H. Sun, H. Wang, B. Yang, *Angew. Chem., Int. Ed.* **2013**, *52*, 3953.
[50] S. Zhu, X. Zhao, Y. Song, S. Lu, B. Yang, *Nano Today* **2016**, *11*, 128.
[51] D. Qu, M. Zheng, L. Zhang, H. Zhao, Z. Xie, X. Jing, R. E. Haddad, H. Fan, Z. Sun, *Sci. Rep.* **2015**, *4*, 5294.
[52] Z.-L. Xu, X.-Y. Wang, M.-Y. Shen, C.-H. Du, *Chem. Pap.* **2016**, *70*, 1649.
[53] T. S. Hansen, J. Mielby, A. Riisager, *Green Chem.* **2011**, *13*, 109.
[54] T. A. Houston, B. L. Wilkinson, J. T. Blanchfield, *Org. Lett.* **2004**, *6*, 679.
[55] X. Hai, J. Feng, X. Chen, J. Wang, *J. Mater. Chem. B* **2018**, *6*, 3219.
[56] F. Ehrat, S. Bhattacharyya, J. Schneider, A. Löf, R. Wyrwich, A. L. Rogach, J. K. Stolarczyk, A. S. Urban, J. Feldmann, *Nano Lett.* **2017**, *17*, 7710.
[57] Y. Xiong, J. Schneider, E. V. Ushakova, A. L. Rogach, *Nano Today* **2018**, *23*, 124.
[58] S. Huang, H. Qiu, S. Lu, F. Zhu, Q. Xiao, *J. Hazard. Mater.* **2015**, *285*, 18.
[59] J. A. Olmstead, D. G. Gray, *J. Pulp Pap. Sci.* **1997**.
[60] T. Ikai, Y. Kojima, K. Shinohara, K. Maeda, S. Kanoh, *Polymer.* **2017**, *117*, 220.
[61] J. He, K. Bian, N. Li, G. Piao, *J. Mater. Chem. C* **2019**, *7*, 9278.

**ADVANCED
SCIENCE NEWS**

www.advancedsciencenews.com

**ADVANCED
OPTICAL
MATERIALS**

www.advopticalmat.de

[62] W. Li, M. Xu, C. Ma, Y. Liu, J. Zhou, Z. Chen, Y. Wang, H. Yu, J. Li, S. Liu, *ACS Appl. Mater. Interfaces* **2019**, *11*, 23512.

[63] Z. Cheng, Y. Ma, L. Yang, F. Cheng, Z. Huang, A. Natan, H. Li, Y. Chen, D. Cao, Z. Huang, Y. H. Wang, Y. Liu, R. Yang, H. Zhu, *Adv. Opt. Mater.* **2019**, *7*, 1801816.

[64] N. Suzuki, Y. C. Wang, P. Elvati, Z.-B. B. Qu, K. Kim, S. Jiang, E. Baumeister, J. J. Lee, B. Yeom, J. H. Bahng, J. J. Lee, A. Violi, N. A. Kotov, *ACS Nano* **2016**, *10*, 1744.

[65] L. Đorđević, F. Arcudi, A. D'Urso, M. Cacioppo, N. Micali, T. Bürgi, R. Purrello, M. Prato, *Nat. Commun.* **2018**, *9*, 3442.

[66] M. Monici, *Biotechnol. Annu. Rev.* **2005**, *11*, 227.

[67] H. Thérien-Aubin, Y. Wang, K. Nothdurft, E. Prince, S. Cho, E. Kumacheva, *Biomacromolecules* **2016**, *17*, 3244.

[68] Y. Li, N. Khuu, A. Gevorkian, S. Sarjinsky, H. Therien-Aubin, Y. Wang, S. Cho, E. Kumacheva, *Angew. Chem., Int. Ed.* **2017**, *56*, 6083.

[69] E. Prince, M. Alizadehgiashi, M. Campbell, N. Khuu, A. Albulescu, K. De France, D. Ratkov, Y. Li, T. Hoare, E. Kumacheva, *Biomacromolecules* **2018**, *19*, 1276.

[70] C. Lemarchand, R. Gref, P. Couvreur, *Eur. J. Pharm. Biopharm.* **2004**, *58*, 327.

[71] P. Decuzzi, B. Godin, T. Tanaka, S.-Y. Lee, C. Chiappini, X. Liu, M. Ferrari, *J. Controlled Release* **2010**, *141*, 320.

[72] K. A. Mahmoud, J. A. Mena, K. B. Male, S. Hrapovic, A. Kamen, J. H. T. Luong, *ACS Appl. Mater. Interfaces* **2010**, *2*, 2924.

[73] S. Cho, Y. Li, M. Seo, E. Kumacheva, *Angew. Chem., Int. Ed.* **2016**, *55*, 14014.

[74] S. Dong, H. J. Cho, Y. W. Lee, M. Roman, *Biomacromolecules* **2014**, *15*, 1560.

[75] M. Guo, S. Her, R. Keunen, S. Zhang, C. Allen, M. A. Winnik, *ACS Omega* **2016**, *1*, 93.

[76] Z. Hosseinidoust, M. N. Alam, G. Sim, N. Tufenkji, T. G. M. van de Ven, *Nanoscale* **2015**, *7*, 16647.

[77] J. A. De La Cruz, Q. Liu, B. Senyuk, A. W. Frazier, K. Peddireddy, I. I. Smalyukh, *ACS Photonics* **2018**, *5*, 2468.

[78] M. G. Debije, P. P. C. Verbunt, *Adv. Energy Mater.* **2012**, *2*, 12.

[79] D. A. Shirley, *Phys. Rev. B* **1972**, *5*, 4709.